

PDTrim: Targeted Pruning for Prefill-Decode Disaggregation in Inference

Hao Zhang*, Mengsi Lyu*, Zhuo Chen, Xingrun Xing, Yulong Ao[†], Yonghua Lin[†]
 Beijing Academy of Artificial Intelligence (BAAI)

Abstract

Large Language Models (LLMs) demonstrate exceptional capabilities across various tasks, but their deployment is constrained by high computational and memory costs. Model pruning provides an effective means to alleviate these demands. However, existing methods often ignore the characteristics of prefill-decode (PD) disaggregation in practice. In this paper, we propose a pruning method that is highly integrated with PD disaggregation, enabling more precise pruning of blocks. Our approach constructs pruning and distillation sets to perform iterative block removal, obtaining better pruning solutions. Moreover, we analyze the pruning sensitivity of the prefill and decode stages and identify removable blocks specific to each stage, making it well suited for PD disaggregation deployment. Extensive experiments demonstrate our approach consistently achieves strong performance in both PD disaggregation and PD unified (non-PD disaggregation) settings, and can also be extended to other non-block pruning methods. Under the same settings, our method achieves improved performance and faster inference.

1 Introduction

Large Language Models (LLMs) have emerged as revolutionary tools, achieving state-of-the-art (SOTA) results across diverse tasks and applications (Ding et al., 2022; Qin et al., 2023; Zhu et al., 2023; Li et al., 2023a). However, the rapid growth in model scale has posed significant challenges for their practical deployment (Zhang et al., 2023; Choi et al., 2025; Long et al., 2025). To address it, various techniques have been proposed, including pruning (Ma et al., 2023; Ashkboos et al., 2024; Li et al., 2023c; Sun et al., 2025), quantization (Liu et al., 2021; Zhou et al., 2023b; Cai et al., 2023;

Zhou et al., 2024) and knowledge distillation (Hinton et al., 2015; Gou et al., 2021; Yang et al., 2021; Zhang et al., 2024). Among them, pruning stands out as an effective strategy for reducing model size by eliminating redundant or less critical components, thereby lowering computational and storage costs.

While pruning offers clear benefits, its application to LLMs remains challenging. During inference, the prefill and decode stages are usually disaggregated (PD disaggregation) (Zhong et al., 2024; Patel et al., 2024; Qin et al., 2024; Dong et al., 2025), allowing each stage to be optimized according to its specific resource requirements. Without such disaggregation, heterogeneous workloads must conform to a single resource profile, which results in suboptimal utilization and ultimately degrades performance. However, existing pruning methods often ignore the characteristics of PD disaggregation deployment in real deployments. In such systems, the prefill and decode stages exhibit markedly different sensitivities to pruning, making uniform strategies ineffective.

In this paper, we propose a pruning method that is highly integrated with PD disaggregation, enabling more precise pruning of blocks. (1) Specifically, we introduce a approach for constructing pruning and distillation sets tailored to block pruning. (2) Building on these sets, we perform an iterative block removal procedure for LLMs. (3) We further analyze the pruning sensitivity of the prefill and decode stages separately, and identify removable blocks specific to each stage. This stage-aware pruning strategy aligns with the distinct execution characteristics of prefill and decode, resulting in particularly efficient PD disaggregation deployment. Compared to prior block pruning approaches, our method achieves better solutions. Extensive experiments demonstrate that our approach consistently achieves strong performance in both PD disaggregation and PD unified (non-PD dis-

*These authors contribute equally to this work.

[†]Corresponding author.

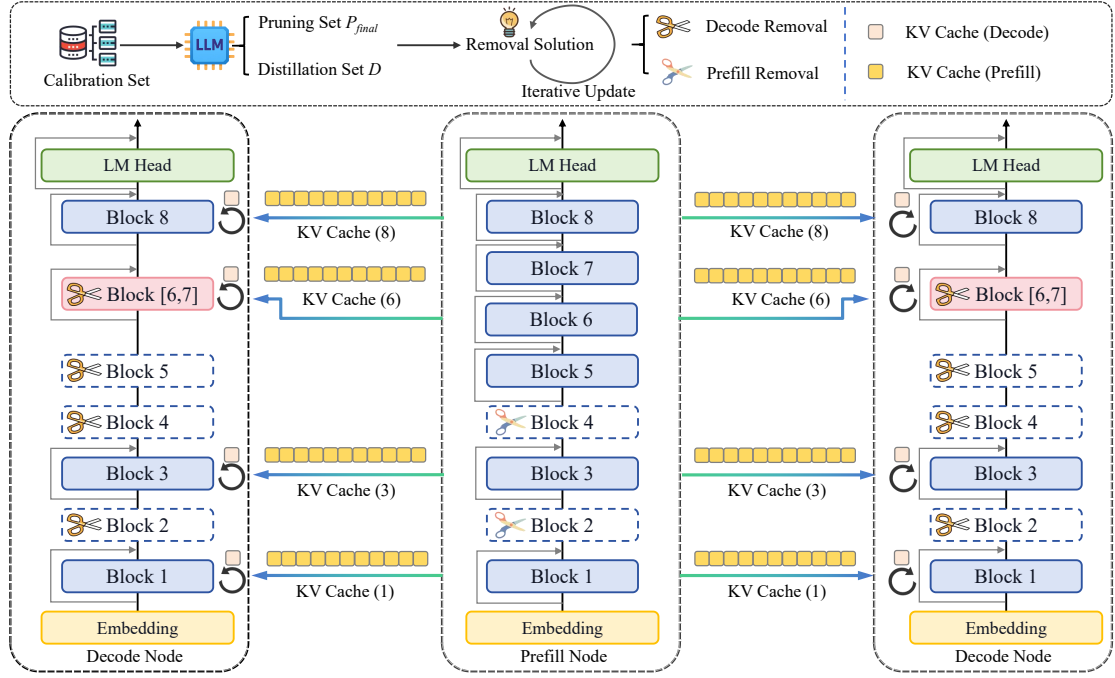


Figure 1: Overview of our pruning method combined with PD disaggregation. Under PD disaggregation, inputs are first processed on the prefill node and then dispatched to multiple decode nodes. The prefill node transfers the KV cache to the decode nodes, while each decode node also generates its own KV cache. In our method, we construct pruning and distillation sets and iteratively optimize the block removal based on these sets. The prefill and decode nodes apply different removal schemes. In this case, the prefill node prunes Blocks 2 and 4, whereas the decode nodes prune Blocks 2, 4 and 5, and further distill Blocks 6 and 7 into a single Block.

aggregation) settings. Our method can also be extended to other non-block pruning scenarios. Under the same settings, our method achieves improved performance and faster inference. In summary, our contributions can be summarized as follows:

- We introduce a construction of pruning and distillation sets for block pruning, and leverage them to perform an iterative block removal strategy for LLMs. This can achieve superior performance over prior methods.
- We analyze the pruning sensitivity of the prefill and decode stages and identify removable blocks specific to each stage, making it well suited for PD disaggregation deployment.
- Our approach consistently achieves strong performance in both PD disaggregation and PD unified (non-PD disaggregation) settings, and can also be extended to other non-block pruning methods.

2 Related Work

2.1 PD Disaggregation

LLM inference can be divided into the prefill and decode stages. The prefill stage processes the entire input sequence to compute contextual representations and generate KV Cache. The decode stage then autoregressively generates tokens conditioned on previously generated outputs. PD disaggregation is a technique that explicitly decouples these two stages during inference, enabling deployment strategies tailored to the unique resource requirements of each stage. DistServe (Zhong et al., 2024) is one of the seminal works in PD disaggregation. It assigns the prefill and decode stages to different GPUs, allowing for optimizations tailored to the unique characteristics of each stage. Splitwise (Patel et al., 2024) disaggregates the prompt computation and token generation stages and runs them on different machines. The TetriInfer (Hu et al., 2024b) also leverages PD disaggregation to reduce interference between different downstream tasks. MemServe (Hu et al., 2024a) further explores memory optimization techniques within the PD disaggregation architecture. TaiChi (Wang et al., 2025)

integrates PD disaggregation and aggregation by leveraging differentiated GPU roles and adaptive scheduling to optimize goodput across diverse SLO regimes. Adrenaline (Liang et al., 2025) offloads part of decode phase attention computation to prefill instances, improving LLM serving.

2.2 Block Pruning

To develop a straightforward pruning algorithm that is easy to deploy for LLMs, several studies have proposed removing less important blocks, a strategy that can lead to significant inference acceleration and improved computational efficiency. For example, methods (Men et al., 2024) using cosine similarity to evaluate block importance combined with greedy pruning have been introduced. However, greedy approaches often fail to identify the globally optimal pruning configuration and tend to exhibit instability in practice. Techniques like LaCo (Yang et al., 2024b) merge subsequent layers into preceding ones but typically sacrifice accuracy compared to direct layer removal. LLM-Streamline (Chen et al., 2024) reduces model size by distilling multiple consecutive blocks into a single block. However, overly aggressive distillation can significantly degrade model performance, and the approach still relies on a greedy block selection strategy. Other methods, such as SLEB (Song et al., 2024) and Shortened LLaMA (Kim et al., 2024), adopt iterative pruning strategies guided by carefully designed importance metrics. However, these methods require recalculating importance scores using a calibration set after each block removal, resulting in substantial computational overhead. Consequently, developing a block pruning algorithm that is highly accurate remains a difficult and unresolved challenge.

3 Methodology

In this section, we describe our iterative block pruning method that is deeply integrated with PD disaggregation. Our goal is to select the k blocks whose removal minimally impacts performance. Figure 1 illustrates an overview of our method.

3.1 Strategic Design of Sets for Pruning and Distillation

We use a combined pruning and distillation strategy for refined block removal. Specifically, we first assess the redundancy of each block by calculating the cosine similarity (Men et al., 2024) between its input and output (note that the similarity metric is

not a core contribution of ours). We provide further details on this in Appendix I. The redundancy of $block_i$ is mathematically defined as follows:

$$r_i = \cos(h_{i-1}, h_i) \quad (1)$$

Here, r_i denotes the redundancy of $block_i$ and the \cos measures the similarity between the input h_{i-1} and the output h_i of $block_i$. Based on this redundancy metric, we directly identify the $Top \lceil \frac{k}{2} \rceil$ blocks with the highest cosine similarity for removal. Given their high redundancy, these blocks are deemed suitable for direct pruning, thereby forming an initial pruning set of $\lceil \frac{k}{2} \rceil$ blocks. The initial pruning set $\mathcal{P}_{initial}$ can be represented as follows:

$$\mathcal{P}_{initial} = \{block_i \mid r_i \in Top \lceil \frac{k}{2} \rceil (\{r_1, r_2, \dots, r_L\})\} \quad (2)$$

For the blocks that are not included in the initial $\lceil \frac{k}{2} \rceil$ blocks designated for pruning, we consider incorporating them into the construction of the distillation set. To ensure the effectiveness of the distillation, we limit distillation to pairs of consecutive blocks. Specifically, for a pair of consecutive blocks, denoted as $block_i$ and $block_{i+1}$, we define a metric d_i to determine whether they should be included in the distillation set. The metric d_i is defined as follows:

$$d_i = \frac{1}{2} (\cos(h_{i-1}, h_{i+1}) + \max(\cos(h_{i-1}, h_i), \cos(h_i, h_{i+1}))) \quad (3)$$

This metric is designed from two complementary perspectives. Here, the $\cos(h_{i-1}, h_{i+1})$ measures redundancy when treating two blocks as a single unit; higher values imply weaker transformation and easier merging. During distillation, we merge consecutive blocks by finetuning the block with lower redundancy and transferring representational capacity from the block with higher redundancy. The more redundant block is identified by $\max(\cos(h_{i-1}, h_i), \cos(h_i, h_{i+1}))$; a larger value indicates higher redundancy and easier capacity transfer. We incorporate a pair of consecutive blocks into the distillation set and distill them into a single block only when the metric d_i exceeds a threshold, denoted as d_T . The distillation set \mathcal{D} can be represented as follows:

$$\mathcal{D} = \{(block_i, block_{i+1}) \mid d_i \geq d_T \text{ and } \{block_i, block_{i+1}\} \cap \mathcal{P}_{initial} = \emptyset\} \quad (4)$$

If a block meets the threshold with both its preceding and succeeding blocks, we select the one

with the higher metric to include in the distillation set. Through this approach, we construct the distillation set, where each element represents the distillation of a pair of consecutive blocks into one block. Once the distillation set is constructed, all blocks not included in it are assigned to the pruning set. The final pruning set \mathcal{P}_{final} can be represented as follows:

$$\mathcal{P}_{final} = \{block_i \mid \{(block_{i-1}, block_i), (block_i, block_{i+1})\} \cap \mathcal{D} = \emptyset\} \quad (5)$$

In this setup, each block in the model is assigned to either the pruning set or the distillation set. Ingeniously, the number of blocks removed by each element in the distillation set matches that in the pruning set, with both strategies removing exactly one block. This consistency establishes a foundation for iterative optimization strategies.

3.2 Iterative Optimization toward Optimal Block Removal

To determine the optimal combination of block removals, we iteratively refine the removal set to minimize the impact on model performance. Specifically, we first initialize the block removal set by selecting the $Top\lceil\frac{k}{2}\rceil$ blocks with the highest cosine similarity from the pruning set. The remaining $k - \lceil\frac{k}{2}\rceil$ blocks $\mathcal{B}_{partial}$ are chosen from the distillation set based on the aforementioned metrics d_i in descending order. If the number of blocks in the distillation set is insufficient, we supplement them from the pruning set in descending order of cosine similarity, excluding the $Top\lceil\frac{k}{2}\rceil$ blocks that need to be pruned. The initial block removal set $\mathcal{B}_{initial}$ can be represented as follows:

$$\mathcal{B}_{partial} = \begin{cases} Top(k - \lceil\frac{k}{2}\rceil)(\mathcal{D}) \\ (if |\mathcal{D}| \geq k - \lceil\frac{k}{2}\rceil) \\ \mathcal{D} \cup Top(k - \lceil\frac{k}{2}\rceil - |\mathcal{D}|)(\mathcal{P}_{final} \setminus \mathcal{P}_{initial}) \\ (if |\mathcal{D}| < k - \lceil\frac{k}{2}\rceil) \end{cases} \quad (6)$$

$$\mathcal{B}_{initial} = \mathcal{P}_{initial} \cup \mathcal{B}_{partial} \quad (7)$$

We define several key parameters for the optimization process. The initial temperature T_0 controls the randomness in the block iteration, the decay coefficient α is employed to gradually reduce the temperature and the termination temperature T_{min} determines when to stop the entire block iteration

(we provide the analysis of these parameters in experiments). In each iteration, we select an element from the unremoved set based on probability to replace a random element in the current removed set, thereby generating a new neighborhood solution. To determine the probability of each element being selected, we assign a weight ω_i to each element i in the unremoved set. For every element i , $block_i$ in the pruning set or element $block_i$ and $block_{i+1}$ in the distillation set, the weight ω_i and the probability p_i are related to formula 1, being selected can be defined as follows:

$$\omega_i = \begin{cases} r_i & pruning\ set \\ \frac{1}{2}(r_i + r_{i+1}) & distillation\ set \end{cases} \quad (8)$$

$$p_i = \frac{\omega_i}{\sum_{j=1}^N \omega_j} \quad (9)$$

Here, N denotes the total number of elements in the unremoved set. For the new candidate block removal solution s' , we calculate its accuracy on the calibration set as the objective function value $f_{s'}$, and compare it with the current solution's (s) objective function value f_s . If the accuracy of the candidate solution is higher ($f_{s'} > f_s$), we directly accept it. However, if the candidate solution's accuracy is lower ($f_{s'} < f_s$), we decide whether to accept it based on a probability. The acceptance probability $P_{s'}$ is calculated using the following formula:

$$P_{s'} = e^{-\frac{\Delta f}{T}} \quad \Delta f = f_s - f_{s'} \quad (10)$$

where Δf is the difference in objective function values between the current solution and the new candidate solution, and T is the current temperature. This probability based acceptance mechanism allows us to escape local optima and explore the solution space more comprehensively. After evaluating the new solution, we update the temperature using the decay factor $T = \alpha T$. We repeat this process until the temperature reaches the minimum threshold T_{min} . Our experiments show that even with fewer iterations, performance still remains strong. Throughout the entire iterative process, we continuously record the block removal combination with the highest performance, considering it as the optimal solution. The optimal solution $\mathcal{B}_{optimal}$ can be represented as follows:

$$\mathcal{B}_{optimal} = \arg \max_{\mathcal{B} \in solutions} f_{\mathcal{B}} \quad (11)$$

where $f_{\mathcal{B}}$ is the objective function value of solution \mathcal{B} . This strategy yields better solutions that

approximate the global optimum, as confirmed by experiments. It requires only a few iterations to achieve improved results, and the partial randomness introduced does not noticeably degrade performance. Moreover, it incurs substantially lower pruning overhead compared to other global search methods, as verified empirically.

3.3 Heterogeneous Strategies Across Prefill and Decode Nodes

The prefill stage is more sensitive to pruning than the decode, pruning during this stage tends to lead to a more significant drop in performance. Here, we provide an abstract analysis, ignoring other complex effects. Denote by $X \in \mathbb{R}^{N \times d}$ the input sequence in the prefill stage and by $x_t \in \mathbb{R}^{1 \times d}$ the initial input in the decode stage. We denote the perturbations of the attention parameters W_Q , W_K and W_V by ΔW_Q , ΔW_K and ΔW_V , respectively. The query vector q and its perturbation Δq for x_t are given by $q = x_t W_Q$ and $\Delta q = x_t \Delta W_Q$. The concatenated key and value matrices are defined as (K, V) , where $K = [K_{pre}, x_t W_K]$ and $V = [V_{pre}, x_t W_V]$, with corresponding perturbations $\Delta K = [\Delta K_{pre}, x_t \Delta W_K]$ and $\Delta V = [\Delta V_{pre}, x_t \Delta W_V]$. Here, $K_{pre} = X W_K$ and $\Delta K = X \Delta W_K$; the same applies to the others. Then, the attention output before (o) and after perturbation (\tilde{o}), as well as the resulting error (E), can be expressed as follows:

$$o = \text{softmax} \left(\frac{qK^\top}{\sqrt{d}} \right) V \quad (12)$$

$$\tilde{o} = \text{softmax} \left(\frac{(q+\Delta q)(K+\Delta K)^\top}{\sqrt{d}} \right) (V + \Delta V) \quad (13)$$

$$\tilde{A} = \text{softmax} \left(\frac{(q+\Delta q)(K+\Delta K)^\top}{\sqrt{d}} \right) \quad (14)$$

$$\Delta A = \tilde{A} - \text{softmax} \left(\frac{qK^\top}{\sqrt{d}} \right) \quad (15)$$

$$E = \tilde{o} - o = \Delta A V + \tilde{A} \Delta V \quad (16)$$

Considering the above analysis, we obtain the following formulas (*The detailed derivation of these formulas can be found in Appendix A and B*):

$$\begin{aligned} \|E\|_F &\leq \frac{L_{\text{softmax}}}{\sqrt{d}} \left(\|\Delta q\|_2 \|K\|_F + \|q\|_2 \right. \\ &\quad \left. \|\Delta K\|_F \right) \cdot \|V\|_F + \|\Delta V\|_F \end{aligned} \quad (17)$$

$$E = G(x_t, Y_{pre}, \Delta) \quad (18)$$

Here, L_{softmax} denotes the Lipschitz constant of the softmax, $\|E\|_F$ denotes the Frobenius norm

of the error E , and G is an abstract error function. Y_{pre} denotes the set of all results (including both intermediate and final outputs) produced in the previous step that can be reused in the current step, and Δ represents the set of perturbations. From this, we observe that pruning errors accumulate as the sequence is generated. During the prefill stage, a perturbation simultaneously contaminates the representations of all N tokens. These corrupted representations are repeatedly accessed in subsequent decode steps, causing the error to accumulate and amplify over time. In contrast, a single decode step only affects the current input and its subsequent states, limiting the scope of impact. Therefore, after determining the optimal combination of removed blocks, we further adjust the removed blocks for each stage. Specifically, for each element in the current combination of removed blocks, we test it on the calibration set. If removing only in the decode stage can significantly improve performance, then that element is removed only in the decode stage while being retained in the prefill stage. If there is no significant performance improvement, then the removing operation for that element will be applied in both the prefill and decode stages. More details can be found in Appendix K and C. This approach allows us to determine the removed blocks for the prefill and the decode separately.

4 Experiments

4.1 Experimental Setup

Models and Benchmarks To demonstrate the effectiveness of our method, we conduct extensive evaluations on representative LLMs with diverse architectures and scales, including LLaMA3.1-8B (Grattafiori et al., 2024), LLaMA2-13B (Touvron et al., 2023), Qwen2.5-7B (Yang et al., 2024a) and Qwen2.5-14B (Yang et al., 2024a). We also use Qwen2.5-32B (Yang et al., 2024a) and OPT-6.7B (Zhang et al., 2022) in the supplementary experiments. We employ a wide range of benchmarks. These benchmarks include MMLU (Hendrycks et al., 2020), CMMLU (Li et al., 2023b), PIQA (Bisk et al., 2020), Winogrande (ai2, 2019), Hellaswag (Zellers et al., 2019), BoolQ (Clark et al., 2019), MathQA (Amini et al., 2019), ARC-Easy and ARC-Challenge (Clark et al., 2018), RTE (Wang et al., 2018), WNLI (Wang et al., 2018), CB (Wang et al., 2019) and SST-2 (Wang et al., 2018). This comprehensive protocol ensures thor-

LLM	Method	MMLU	CMMLU	ARC-E	ARC-C	PIQA	Winog	HSwag	BoolQ	MathQA	WNLI	SST-2	RTE	CB	Avg
LLaMA3.1-8B	Dense	63.35	50.85	81.52	51.28	80.30	74.03	60.05	82.26	39.56	59.15	76.83	71.12	60.71	65.46
	LLM-Pruner	52.01	41.12	67.36	42.06	74.54	69.32	51.50	73.78	32.35	50.78	69.37	49.40	55.28	56.07
	FLAP	52.11	41.13	67.42	42.15	74.63	69.36	51.56	73.82	32.39	50.82	69.41	49.44	55.34	56.11
	Shortened	33.54	34.28	72.31	42.15	72.63	69.61	47.96	45.23	34.27	56.34	52.52	67.15	69.64	53.66
	ShortGPT	51.92	41.11	67.34	42.06	74.48	69.38	51.56	73.76	32.50	50.70	69.31	49.50	55.36	56.08
	SLEB	28.35	25.51	71.04	36.18	75.46	62.98	49.70	57.89	27.30	46.48	55.85	57.04	35.71	48.42
	Ours	60.82	46.66	73.15	43.86	76.99	73.56	53.80	69.85	34.28	60.56	83.03	70.76	73.21	62.99
LLaMA2-13B	Dense	52.10	34.73	79.42	48.38	79.05	72.22	60.07	80.61	32.09	66.20	87.61	69.31	80.36	64.78
	LLM-Pruner	50.11	33.57	61.16	37.67	71.38	70.71	47.37	62.53	24.41	43.24	65.37	59.19	51.38	52.16
	FLAP	49.89	33.91	60.90	37.65	71.44	70.69	47.54	62.43	24.78	43.26	64.91	59.19	51.34	52.15
	Shortened	26.71	25.50	26.26	22.61	51.14	48.22	25.76	38.93	18.89	43.66	46.56	52.71	37.50	35.73
	ShortGPT	50.13	33.97	61.32	37.88	71.44	70.80	47.71	62.54	24.82	43.66	65.37	59.57	51.79	52.38
	SLEB	23.76	25.41	67.85	33.87	75.41	63.77	48.76	62.42	25.46	45.07	50.92	58.84	41.07	47.89
	Ours	51.52	35.37	69.78	40.02	74.43	70.72	53.11	62.84	28.44	53.52	80.16	64.26	46.43	56.20
Qwen2.5-7B	Dense	71.92	81.69	80.56	48.21	78.73	72.93	59.92	84.46	43.22	71.83	91.86	81.23	87.50	73.39
	LLM-Pruner	36.96	36.71	71.33	38.20	74.86	55.79	47.71	55.67	31.08	60.43	70.79	54.42	38.81	51.75
	FLAP	37.17	36.39	71.47	37.83	76.21	55.65	47.47	57.23	30.11	61.61	70.68	54.59	37.32	51.82
	Shortened	24.90	25.08	25.25	20.31	53.65	50.99	25.69	37.83	19.50	53.52	50.92	46.21	19.64	34.88
	ShortGPT	36.89	31.07	71.46	37.80	76.12	55.80	48.67	63.21	30.59	42.25	80.62	54.87	41.07	51.57
	SLEB	38.56	38.25	71.84	39.42	76.77	55.96	47.98	57.49	31.12	61.97	72.25	56.32	39.29	52.86
	Ours	52.96	51.34	71.09	39.16	77.04	56.99	51.19	72.20	30.95	66.20	63.53	65.34	57.14	58.09
Qwen2.5-14B	Dense	77.45	84.44	82.37	56.31	81.12	75.37	63.37	85.23	53.03	77.46	89.11	79.78	80.36	75.80
	LLM-Pruner	43.09	42.01	73.33	40.54	73.58	58.47	47.79	61.89	31.53	48.79	54.26	56.88	49.27	52.42
	FLAP	44.86	44.77	50.29	31.00	60.72	51.44	34.14	65.16	25.65	65.28	89.95	76.87	68.74	54.53
	Shortened	24.63	25.31	25.04	20.14	52.88	50.43	25.69	37.92	18.93	52.11	48.62	51.99	37.50	36.25
	ShortGPT	45.75	45.63	50.63	31.40	61.81	52.64	34.41	65.72	26.16	66.20	91.28	78.34	69.64	55.35
	SLEB	43.77	42.90	74.07	41.04	74.37	58.96	48.43	62.57	32.23	49.30	54.93	57.40	50.00	53.07
	Ours	72.01	76.82	68.81	44.37	71.38	70.17	47.98	64.80	34.91	61.97	82.11	74.01	69.65	64.54

Table 1: Performance comparison of pruning methods in LLMs across a variety of benchmarks. To increase the diversity of evaluation, we apply pruning rates of 13.6%, 24.4%, 15.3% and 18.6% for the four models, corresponding to commonly used pruning ratios for structured pruning.

ough assessment.

Baselines We conduct comparative evaluations against other methods, including LLM-Pruner (Ma et al., 2023), FLAP (An et al., 2024), Shortened LLaMA (abbreviated as Shortened)(Kim et al., 2024), ShortGPT (Men et al., 2024) and SLEB (Song et al., 2024). Additionally, we also use SliceGPT (Ashkboos et al., 2024) to test inference speed. We implement PD disaggregation versions of the classic channel pruning LLM-Pruner and block pruning ShortGPT according to our algorithm, and use them as additional baselines. More details can be found in Appendix C.

Implementation Details Our experiments are conducted using the PyTorch framework (Paszke et al., 2019) and the Hugging Face Transformers library (Wolf et al., 2020). We use two nodes, each equipped with one NVIDIA H100 80GB GPU. When distilling two blocks, we use the weights of the block with low cosine similarity as the initial weights. By default, we use 256 randomly sampled examples from PIQA and MMLU as the calibration set. The hyperparameter settings and training details can be found in Appendix C.

4.2 Main Results

We evaluate our method against strong baselines on four representative LLMs and multiple benchmarks under identical experimental settings, including the calibration set. To diversify the evaluation, we adopt pruning ratios of 13.6%, 24.4%, 15.3% and 18.6% across the four models. The Dense configuration corresponds to the original uncompressed model, serving as a reference prior to pruning. The experiments are conducted with consistent parameter settings and implementation details. As shown in Table 1, our method consistently outperforms all baselines across different models. These results clearly confirm the effectiveness and robustness of our method under diverse pruning scenarios.

Our approach serves as an optimization for PD disaggregation and can be readily combined with other pruning methods. We extend two representative approaches, the channel pruning method LLM-Pruner and the block pruning method ShortGPT. Specifically, we first use LLM-Pruner and ShortGPT to select pruning weights for the decode stage, and then apply our method to identify a pruned subset of weights for the prefill stage. The resulting approaches are denoted as LLM-Pruner (Ours) and

LLM	Method	MMLU	CMMLU	ARC-E	ARC-C	HSwag	MathQA	WNLI	RTE	Avg
LLaMA3.1-8B	LLM-Pruner	52.01	41.12	67.36	42.06	51.50	32.35	50.78	49.40	48.32
	ShortGPT	51.92	41.11	67.34	42.06	51.56	32.50	50.70	49.50	48.34
	LLM-Pruner (Ours)	54.95	44.30	72.46	43.82	52.84	34.13	53.94	52.88	51.16
	ShortGPT (Ours)	54.62	43.89	71.38	43.11	53.55	35.08	53.62	52.63	50.98
	Ours	60.82	46.66	73.15	43.86	53.80	34.28	60.56	70.76	55.49
	LLM-Pruner	50.11	33.57	61.16	37.67	47.37	24.41	43.24	59.19	44.59
LLaMA2-13B	ShortGPT	50.13	33.97	61.32	37.88	47.71	24.82	43.66	59.57	44.88
	LLM-Pruner (Ours)	52.58	34.27	65.55	39.19	49.99	25.96	44.53	62.54	46.83
	ShortGPT (Ours)	53.70	34.28	64.25	38.98	50.76	26.50	46.84	63.41	47.34
Qwen2.5-7B	Ours	51.52	35.37	69.78	40.02	53.11	28.44	53.52	64.26	49.50
	LLM-Pruner	36.96	36.71	71.33	38.20	47.71	31.08	60.43	54.42	47.11
	ShortGPT	36.89	31.07	71.46	37.80	48.67	30.59	42.25	54.87	44.20
Qwen2.5-14B	LLM-Pruner (Ours)	38.99	39.42	72.41	38.66	50.54	33.34	61.89	56.83	49.01
	ShortGPT (Ours)	39.51	33.01	73.04	39.01	51.18	32.88	62.96	56.64	48.53
	Ours	52.96	51.34	71.09	39.16	51.19	30.95	66.20	65.34	53.53
Qwen2.5-14B	LLM-Pruner	43.09	42.01	73.33	40.54	47.79	31.53	48.79	56.88	48.00
	ShortGPT	45.75	45.63	50.63	31.40	34.41	26.16	66.20	78.34	47.32
	LLM-Pruner (Ours)	65.75	45.32	74.49	43.13	48.75	32.43	51.27	58.44	52.45
Qwen2.5-14B	ShortGPT (Ours)	68.34	47.36	52.21	33.16	36.37	28.05	67.64	78.89	51.50
	Ours	72.01	76.82	68.81	44.37	47.98	34.91	61.97	74.01	60.11

Table 2: Performance comparison of our method with LLM-Pruner and ShortGPT, as well as their variants. LLM-Pruner (Ours) and ShortGPT (Ours) are our PD disaggregation extensions.

ShortGPT (Ours), respectively. As shown in Table 2, both methods exhibit substantial performance improvements on the evaluated datasets after applying PD disaggregation. Moreover, our approach consistently achieves the best overall results. These findings highlight the effectiveness of PD disaggregation as a general principle for enhancing pruning strategies in LLMs. To validate the scalability and generality of our method, we conduct experiments on larger model, additional datasets, and an extra metric (perplexity), achieving promising results (see Appendix D).

4.3 Efficiency Analysis

Inference Latency We measure the execution time for a single inference of the LLaMA3.1-8B model with an input tensor of shape [1, 1024] in FP32 format. Specifically, we evaluate the effects of pruning 13.58% and approximately 50% of the parameters in LLaMA3.1-8B. We then compare our proposed method against several other widely used pruning algorithms, including SliceGPT, LLM-Pruner and FLAP. As shown in Table 3, our approach consistently achieves the fastest runtime, significantly reducing inference latency. This demonstrates that our block pruning approach enables faster inference speed.

Method	Dense	SliceGPT	LLM-Pruner	FLAP	Ours
Time (13.58%)	287.35	263.35	278.19	259.81	236.63
Time (~50%)	287.35	202.69	252.69	184.16	151.89

Table 3: Comparison of inference time (ms) for the LLaMA3.1-8B on different pruning methods.

Pruning Overhead We conduct a comparison of the computational overhead between our proposed pruning method and SLEB. SLEB (Song et al., 2024) is also a pruning strategy that aims to identify the optimal pruning solution. We prune five blocks on LLaMA3.1-8B. The hyperparameters we use have been provided in the experiment details in the previous section. As shown in Table 4, our method achieves an average runtime of only 44.06 seconds, whereas SLEB requires 183.6 seconds on average. Moreover, we conduct a comparison of pruning overhead on LLaMA2-13B under a pruning rate of 24.4%, where our approach continues to demonstrate a significant advantage. This efficiency improvement is attributed to our iterative pruning strategy, which can more rapidly converge to an effective pruning configuration.

4.4 Evaluation in the PD Unified Setting

We compare the performance of our method with other approaches in the non-PD disaggregation setting, referred to as PD Unified. In this setting, the

Model	Method	Pruning Time (s)
LLaMA3.1-8B	SLEB (Song et al., 2024)	183.6
	Ours	44.06
LLaMA2-13B	SLEB (Song et al., 2024)	858.12
	Ours	96.52

Table 4: Comparison of pruning time between our method and SLEB on LLaMA series models.

prefill and decode stages are not explicitly disaggregated during inference. Specifically, we evaluate our method on the LLaMA2-13B model with 24.4% of its parameters pruned across multiple benchmarks. As shown in Table 5, our approach continues to achieve strong and consistent performance in the PD Unified scenario. These results demonstrate that, even without explicit disaggregation of the prefill and decode stages, our method maintains performance across diverse tasks.

4.5 Comparison between Disaggregation and Unified

To validate the effectiveness of our strategy, we conduct extensive benchmarks on LLaMA2-13B by pruning 24.4% of the model parameters. As a baseline, PD Unified applies the same parameter removal configuration to both the prefill and decode stages, without accounting for their differing sensitivities to pruning. As shown in Table 6, our PD disaggregation compression strategy consistently outperforms the PD unified baseline across benchmarks. These results provide strong evidence for the effectiveness of PD disaggregation pruning.

4.6 Orthogonal to Quantization

To evaluate the compatibility and effectiveness of our method under combined compression strategies, we further integrate it with quantization techniques. Specifically, we apply our approach to the Qwen2.5-32B with a pruning ratio of 25% in conjunction with 8-bit AWQ quantization (Lin et al., 2024). As shown in Table 7, our method consistently demonstrates robust performance, indicating that the pruning strategy is largely orthogonal to quantization and can be effectively combined without significant degradation.

5 Conclusion

In this paper, we propose a pruning method that is deeply integrated with PD disaggregation. In particular, we construct pruning and distillation sets to perform iterative block removal, indepen-

dently tailored to the prefill and decode, achieving better solutions compared to prior block pruning approaches. Moreover, we analyze the pruning sensitivity of the prefill and decode stages and identify removable blocks specific to each stage, making it well suited for PD disaggregation deployment. Under the same settings, our method achieves improved performance and faster inference. Extensive experiments demonstrate our approach consistently achieves strong performance in both PD disaggregation and PD unified (non-PD disaggregation) settings, and can also be extended to other non-block pruning methods.

Limitations

In this work, we conduct extensive experiments to evaluate the effectiveness of our pruning method. The results demonstrate that our approach achieves competitive performance compared to the baselines. However, due to computational constraints, we have not yet been able to evaluate it on larger scale models, such as those with 70 billion parameters. Exploring the scalability of our method to such large models constitutes an important direction for future work.

References

2019. Winogrande: An adversarial winograd schema challenge at scale.

Aida Amini, Saadia Gabriel, Peter Lin, Rik Koncel-Kedziorski, Yejin Choi, and Hannaneh Hajishirzi. 2019. Mathqa: Towards interpretable math word problem solving with operation-based formalisms. *arXiv preprint arXiv:1905.13319*.

Yongqi An, Xu Zhao, Tao Yu, Ming Tang, and Jinqiao Wang. 2024. Fluctuation-based adaptive structured pruning for large language models. In *Proceedings of the AAAI Conference on Artificial Intelligence*, volume 38, pages 10865–10873.

Saleh Ashkboos, Maximilian L Croci, Marcelo Gennari do Nascimento, Torsten Hoefer, and James Hensman. 2024. SliceGPT: Compress large language models by deleting rows and columns. *arXiv preprint arXiv:2401.15024*.

Yonatan Bisk, Rowan Zellers, Jianfeng Gao, Yejin Choi, and 1 others. 2020. Piqa: Reasoning about physical commonsense in natural language. In *Proceedings of the AAAI conference on artificial intelligence*, volume 34, pages 7432–7439.

Yuchen Cai, Zhen Wang, Yujun Li, Sheng Wang, Zhiyuan Liu, and Maosong Sun. 2023. Gptq:

Method	MMLU	CMMLU	ARC-E	ARC-C	HSwag	MathQA	WNLI	RTE	AVG
Dense	52.10	34.73	79.42	48.38	60.07	32.09	66.20	69.31	55.29
LLM-Pruner	50.11	33.57	61.16	37.67	47.37	24.41	43.24	59.19	44.59
FLAP	49.89	33.91	60.90	37.65	47.54	24.78	43.26	59.19	44.64
Shortened	26.71	25.50	26.26	22.61	25.76	18.89	43.66	52.71	30.26
ShortGPT	50.13	33.97	61.32	37.88	47.71	24.82	43.66	59.57	44.88
SLEB	23.76	25.41	67.85	33.87	48.76	25.46	45.07	58.84	41.13
Ours (Unified)	51.05	33.99	64.02	37.88	48.83	26.06	53.12	63.54	47.31

Table 5: Evaluation of pruning performance in the PD Unified scenario with LLaMA2-13B.

Strategy	MMLU	CMMLU	ARC-E	ARC-C	HSwag	MathQA	WNLI	RTE	AVG
Unified	51.05	33.99	64.02	37.88	48.83	26.06	53.12	63.54	47.31
Disaggregation	51.52	35.37	69.78	40.02	53.11	28.44	53.52	64.26	49.50

Table 6: Performance comparison between PD Unified and PD Disaggregation on LLaMA2-13B.

Method	PIQA	Winog	HellaSwag	ARC-E	ARC-C
Dense	81.88	75.3	64.91	80.51	53.41
FLAP	77.56	61.08	55.23	70.36	42.37
Ours	78.45	72.85	57	75.8	46.67
Ours + Quant	78.21	71.98	56.88	75.21	46.1

Table 7: Performance of our pruning method with 8-bit AWQ quantization on Qwen2.5-32B.

Accurate post-training quantization for generative pre-trained transformers. *arXiv preprint arXiv:2302.06557*.

Mark Chen, Jerry Tworek, Heewoo Jun, Qiming Yuan, Henrique Ponde De Oliveira Pinto, Jared Kaplan, Harri Edwards, Yuri Burda, Nicholas Joseph, Greg Brockman, and 1 others. 2021. Evaluating large language models trained on code. *arXiv preprint arXiv:2107.03374*.

Xiaodong Chen, Yuxuan Hu, Jing Zhang, Yanling Wang, Cuiping Li, and Hong Chen. 2024. Streamlining redundant layers to compress large language models. *arXiv preprint arXiv:2403.19135*.

Seonghwan Choi, Beomseok Kang, Dongwon Jo, and Jae-Joon Kim. 2025. Retrospective sparse attention for efficient long-context generation. *arXiv preprint arXiv:2508.09001*.

Christopher Clark, Kenton Lee, Ming-Wei Chang, Tom Kwiatkowski, Michael Collins, and Kristina Toutanova. 2019. Boolq: Exploring the surprising difficulty of natural yes/no questions. *arXiv preprint arXiv:1905.10044*.

Peter Clark, Isaac Cowhey, Oren Etzioni, Tushar Khot, Ashish Sabharwal, Carissa Schoenick, and Oyvind Tafjord. 2018. Think you have solved question answering? try arc, the ai2 reasoning challenge. *arXiv preprint arXiv:1803.05457*.

G. Ding and 1 others. 2022. Efficient fine-tuning for resource-constrained systems. *Proceedings of the Machine Learning Conference*.

Xianzhe Dong, Tongxuan Liu, Yuting Zeng, Liangyu Liu, Yang Liu, Siyu Wu, Yu Wu, Hailong Yang, Ke Zhang, and Jing Li. 2025. Hydrainfer: Hybrid disaggregated scheduling for multimodal large language model serving. *arXiv preprint arXiv:2505.12658*.

Jianping Gou, Baosheng Yu, Stephen J Maybank, and Dacheng Tao. 2021. Knowledge distillation: A survey. *International journal of computer vision*, 129(6):1789–1819.

Aaron Grattafiori, Abhimanyu Dubey, Abhinav Jauhri, Abhinav Pandey, Abhishek Kadian, Ahmad Al-Dahle, Aiesha Letman, Akhil Mathur, Alan Schelten, Alex Vaughan, and 1 others. 2024. The llama 3 herd of models. *arXiv preprint arXiv:2407.21783*.

Dan Hendrycks, Collin Burns, Steven Basart, Andy Zou, Mantas Mazeika, Dawn Song, and Jacob Steinhardt. 2020. Measuring massive multitask language understanding. *arXiv preprint arXiv:2009.03300*.

Geoffrey Hinton, Oriol Vinyals, and Jeff Dean. 2015. Distilling the knowledge in a neural network. *arXiv preprint arXiv:1503.02531*.

Cunchen Hu, Heyang Huang, Junhao Hu, Jiang Xu, Xusheng Chen, Tao Xie, Chenxi Wang, Sa Wang, Yungang Bao, Ninghui Sun, and 1 others. 2024a. Memserve: Context caching for disaggregated llm serving with elastic memory pool. *arXiv preprint arXiv:2406.17565*.

Cunchen Hu, Heyang Huang, Liangliang Xu, Xusheng Chen, Jiang Xu, Shuang Chen, Hao Feng, Chenxi Wang, Sa Wang, Yungang Bao, and 1 others. 2024b. Inference without interference: Disaggregate llm inference for mixed downstream workloads. *arXiv preprint arXiv:2401.11181*.

Bo-Kyeong Kim, Geonmin Kim, Tae-Ho Kim, Thibault Castells, Shinkook Choi, Junho Shin, and Hyoung-Kyu Song. 2024. Shortened llama: A simple depth pruning for large language models. *arXiv preprint arXiv:2402.02834*, 11.

C. Li and 1 others. 2023a. Fine-tuning techniques for efficient model adaptation. *AI Research Journal*.

Haonan Li, Yixuan Zhang, Fajri Koto, Yifei Yang, Hai Zhao, Yeyun Gong, Nan Duan, and Timothy Baldwin. 2023b. Cmmlu: Measuring massive multitask language understanding in chinese. *arXiv preprint arXiv:2306.09212*.

Yong Li, Wei Du, Liquan Han, Zhenjian Zhang, and Tongtong Liu. 2023c. A communication-efficient, privacy-preserving federated learning algorithm based on two-stage gradient pruning and differentiated differential privacy. *Sensors*, 23(23):9305.

Yunkai Liang, Zhangyu Chen, Pengfei Zuo, Zhi Zhou, Xu Chen, and Zhou Yu. 2025. Injecting adrenaline into llm serving: Boosting resource utilization and throughput via attention disaggregation. *arXiv preprint arXiv:2503.20552*.

Ji Lin, Jiaming Tang, Haotian Tang, Shang Yang, Wei-Ming Chen, Wei-Chen Wang, Guangxuan Xiao, Xingyu Dang, Chuang Gan, and Song Han. 2024. Awq: Activation-aware weight quantization for on-device llm compression and acceleration. *Proceedings of machine learning and systems*, 6:87–100.

Zhenhua Liu, Yunhe Wang, Kai Han, Wei Zhang, Siwei Ma, and Wen Gao. 2021. Post-training quantization for vision transformer. *Advances in Neural Information Processing Systems*, 34:28092–28103.

Lingkun Long, Rubing Yang, Yushi Huang, Desheng Hui, Ao Zhou, and Jianlei Yang. 2025. Sliminfer: Accelerating long-context llm inference via dynamic token pruning. *arXiv preprint arXiv:2508.06447*.

Xinyin Ma, Gongfan Fang, and Xinchao Wang. 2023. Llm-pruner: On the structural pruning of large language models. *Advances in neural information processing systems*, 36:21702–21720.

Xin Men, Mingyu Xu, Qingyu Zhang, Bingning Wang, Hongyu Lin, Yaojie Lu, Xianpei Han, and Weipeng Chen. 2024. Shortgpt: Layers in large language models are more redundant than you expect. *arXiv preprint arXiv:2403.03853*.

Saurav Muralidharan, Sharath Turuvekere Sreenivas, Raviraj Joshi, Marcin Chochowski, Mostofa Patwary, Mohammad Shoeybi, Bryan Catanzaro, Jan Kautz, and Pavlo Molchanov. 2024. Compact language models via pruning and knowledge distillation. *Advances in Neural Information Processing Systems*, 37:41076–41102.

Adam Paszke, Sam Gross, Francisco Massa, Adam Lerer, James Bradbury, Gregory Chanan, Trevor Killeen, Zeming Lin, Natalia Gimelshein, Luca Antiga, and 1 others. 2019. Pytorch: An imperative style, high-performance deep learning library. *Advances in neural information processing systems*, 32.

Pratyush Patel, Esha Choukse, Chaojie Zhang, Aashaka Shah, Íñigo Goiri, Saeed Maleki, and Ricardo Bianchini. 2024. Splitwise: Efficient generative llm inference using phase splitting. In *2024 ACM/IEEE 51st Annual International Symposium on Computer Architecture (ISCA)*, pages 118–132. IEEE.

A. Qin and 1 others. 2023. Advances in state-of-the-art natural language processing. *Journal of NLP Research*.

Ruoyu Qin, Zheming Li, Weiran He, Mingxing Zhang, Yongwei Wu, Weimin Zheng, and Xinran Xu. 2024. Mooncake: A kvcache-centric disaggregated architecture for llm serving. *arXiv preprint arXiv:2407.00079*.

Jiwon Song, Kyungseok Oh, Taesu Kim, Hyungjun Kim, Yulhwa Kim, and Jae-Joon Kim. 2024. Sleb: Streamlining llms through redundancy verification and elimination of transformer blocks. *arXiv preprint arXiv:2402.09025*.

Weigao Sun, Jiaxi Hu, Yucheng Zhou, Jusen Du, Disen Lan, Kexin Wang, Tong Zhu, Xiaoye Qu, Yu Zhang, Xiaoyu Mo, and 1 others. 2025. Speed always wins: A survey on efficient architectures for large language models. *arXiv preprint arXiv:2508.09834*.

Hugo Touvron, Louis Martin, Kevin Stone, Peter Albert, Amjad Almahairi, Yasmine Babaei, Nikolay Bashlykov, Soumya Batra, Prajjwal Bhargava, Shruti Bhosale, and 1 others. 2023. Llama 2: Open foundation and fine-tuned chat models. *arXiv preprint arXiv:2307.09288*.

Alex Wang, Yada Pruksachatkun, Nikita Nangia, Amanpreet Singh, Julian Michael, Felix Hill, Omer Levy, and Samuel Bowman. 2019. Super glue: A stickier benchmark for general-purpose language understanding systems. *Advances in neural information processing systems*, 32.

Alex Wang, Amanpreet Singh, Julian Michael, Felix Hill, Omer Levy, and Samuel R Bowman. 2018. Glue: A multi-task benchmark and analysis platform for natural language understanding. *arXiv preprint arXiv:1804.07461*.

Chao Wang, Pengfei Zuo, Zhangyu Chen, Yunkai Liang, Zhou Yu, and Ming-Chang Yang. 2025. Prefill-decode aggregation or disaggregation? unifying both for goodput-optimized llm serving. *arXiv preprint arXiv:2508.01989*.

Thomas Wolf, Lysandre Debut, Victor Sanh, Julien Chaumond, Clement Delangue, Anthony Moi, Pieric Cistac, Tim Rault, Rémi Louf, Morgan Funtowicz, and 1 others. 2020. Transformers: State-of-the-art natural language processing. In *Proceedings of the 2020 conference on empirical methods in natural*

language processing: system demonstrations, pages 38–45.

An Yang, Baosong Yang, Beichen Zhang, Binyuan Hui, Bo Zheng, Bowen Yu, Chengyuan Li, Dayiheng Liu, Fei Huang, Haoran Wei, and 1 others. 2024a. Qwen2. 5 technical report. *arXiv preprint arXiv:2412.15115*.

Yifei Yang, Zouying Cao, and Hai Zhao. 2024b. Laco: Large language model pruning via layer collapse. *arXiv preprint arXiv:2402.11187*.

Zhen Yang, Zilun Zhang, Sheng Wang, Jie Li, Meishan Zhang, Zhiyuan Liu, and Maosong Sun. 2021. Knowledge distillation: A survey. *arXiv preprint arXiv:2106.05860*.

Rowan Zellers, Ari Holtzman, Yonatan Bisk, Ali Farhadi, and Yejin Choi. 2019. Hellaswag: Can a machine really finish your sentence? *arXiv preprint arXiv:1905.07830*.

D. Zhang and 1 others. 2023. Parameter-efficient fine-tuning methods for llms. *Journal of Machine Learning Research*.

Qifan Zhang, Yunhui Guo, and Yu Xiang. 2024. **Continual distillation learning: Knowledge distillation in prompt-based continual learning.** *Preprint*, arXiv:2407.13911.

Susan Zhang, Stephen Roller, Naman Goyal, Mikel Artetxe, Moya Chen, Shuhui Chen, Christopher Deewani, Mona Diab, Xian Li, Xi Victoria Lin, and 1 others. 2022. Opt: Open pre-trained transformer language models. *arXiv preprint arXiv:2205.01068*.

Yinmin Zhong, Shengyu Liu, Junda Chen, Jianbo Hu, Yibo Zhu, Xuanzhe Liu, Xin Jin, and Hao Zhang. 2024. {DistServe}: Disaggregating prefill and decoding for goodput-optimized large language model serving. In *18th USENIX Symposium on Operating Systems Design and Implementation (OSDI 24)*, pages 193–210.

Jeffrey Zhou, Tianjian Lu, Swaroop Mishra, Siddhartha Brahma, Sujoy Basu, Yi Luan, Denny Zhou, and Le Hou. 2023a. Instruction-following evaluation for large language models. *arXiv preprint arXiv:2311.07911*.

Yuxiao Zhou, Zhen Wang, Yujun Li, Sheng Wang, Zhiyuan Liu, and Maosong Sun. 2023b. Smoothquant: Accurate and efficient post-training quantization for large language models. *arXiv preprint arXiv:2302.06557*.

Yuxiao Zhou, Zhen Wang, Yujun Li, Sheng Wang, Zhiyuan Liu, and Maosong Sun. 2024. Framequant: Flexible low-bit quantization for transformers. *arXiv preprint arXiv:2402.06557*.

B. Zhu and 1 others. 2023. Large language models: Progress and applications. *Advances in NLP*.

A Detailed Derivation of the Theoretical Formula

Denote by $X \in \mathbb{R}^{N \times d}$ the input sequence in the prefill stage and by $x_t \in \mathbb{R}^{1 \times d}$ the initial input in the decode stage. We denote the perturbations of the attention parameters W_Q , W_K and W_V by ΔW_Q , ΔW_K and ΔW_V , respectively. The query vector q and its perturbation Δq for x_t are as follows:

$$q = x_t W_Q, \quad \Delta q = x_t \Delta W_Q \quad (19)$$

The concatenated key and value matrices (K, V) , along with their perturbations $(\Delta K, \Delta V)$, can be represented as follows:

$$K = [K_{pre}, x_t W_K], \quad V = [V_{pre}, x_t W_V] \quad (20)$$

$$\Delta K = [\Delta K_{pre}, x_t \Delta W_K], \quad \Delta V = [\Delta V_{pre}, x_t \Delta W_V] \quad (21)$$

Here, $K_{pre} = X W_K$ and $\Delta K = X \Delta W_K$; the same applies to the others. Then, the attention output before (o) and after perturbation (\tilde{o}), as well as the resulting error (E), can be expressed as follows:

$$o = \text{softmax} \left(\frac{q K^\top}{\sqrt{d}} \right) V \quad (22)$$

$$\tilde{o} = \text{softmax} \left(\frac{(q + \Delta q)(K + \Delta K)^\top}{\sqrt{d}} \right) (V + \Delta V) \quad (23)$$

$$\tilde{A} = \text{softmax} \left(\frac{(q + \Delta q)(K + \Delta K)^\top}{\sqrt{d}} \right) \quad (24)$$

$$\Delta A = \tilde{A} - \text{softmax} \left(\frac{q K^\top}{\sqrt{d}} \right) \quad (25)$$

$$E = \tilde{o} - o = \Delta A V + \tilde{A} \Delta V \quad (26)$$

To bound the Frobenius norm of the attention output perturbation E , we apply the triangle inequality to separate the contributions from the two terms, yielding the following expression:

$$\|E\|_F \leq \|\Delta A V\|_F + \|\tilde{A} \Delta V\|_F \quad (27)$$

Then, using the submultiplicativity of matrix norms, we can directly obtain the following bounds:

$$\|\Delta A V\|_F \leq \|\Delta A\|_F \|V\|_F \quad (28)$$

$$\|\tilde{A} \Delta V\|_F \leq \|\tilde{A}\|_2 \|\Delta V\|_F \quad (29)$$

By the Lipschitz continuity of the softmax, the perturbation ΔA can naturally be bounded as follows:

$$\|\Delta A\|_F \leq L_{\text{softmax}} \frac{\|(q + \Delta q)(K + \Delta K)^\top - q K^\top\|_F}{\sqrt{d}} \quad (30)$$

Here, L_{softmax} is the Lipschitz constant of the softmax. Upon expanding the product, we can explicitly obtain the resulting expression as follows:

$$\begin{aligned} & (q + \Delta q)(K + \Delta K)^\top - q K^\top \\ &= \Delta q K^\top + q (\Delta K)^\top + (\Delta q)(\Delta K)^\top \end{aligned} \quad (31)$$

where the last term $(\Delta q)(\Delta K)^\top$ is of second order and can be neglected in a first order analysis. Applying the submultiplicativity of the Frobenius norm, we can further obtain the following bounds:

$$\|\Delta q K^\top\|_F \leq \|\Delta q\|_2 \|K\|_F \quad (32)$$

$$\|q(\Delta K)^\top\|_F \leq \|q\|_2 \|\Delta K\|_F \quad (33)$$

Considering all above analysis, we can express the Frobenius norm of the error E as follows:

$$\begin{aligned} \|E\|_F &\leq \frac{L_{\text{softmax}}}{\sqrt{d}} \left(\|\Delta q\|_2 \|K\|_F + \|q\|_2 \right. \\ &\quad \left. \|\Delta K\|_F \right) \|V\|_F + \|\tilde{A}\|_2 \|\Delta V\|_F \end{aligned} \quad (34)$$

Considering that $\|\tilde{A}\|_2 \leq 1$, we obtain the following expression:

$$\begin{aligned} \|E\|_F &\leq \frac{L_{\text{softmax}}}{\sqrt{d}} \left(\|\Delta q\|_2 \|K\|_F + \|q\|_2 \right. \\ &\quad \left. \|\Delta K\|_F \right) \cdot \|V\|_F + \|\Delta V\|_F \end{aligned} \quad (35)$$

Building on the above formula, and to more clearly illustrate the effect of pruning, we can express the error E at step t using an abstract error function G as follows:

$$E = G(x_t, Y_{pre}, \Delta) \quad (36)$$

where Y_{pre} denotes the set of all results (including both intermediate and final outputs) produced in the previous step that can be reused in the current step, and Δ represents the set of perturbations.

B Frobenius Norm of ΔA via Softmax Lipschitz Continuity

For any $a, b \in \mathbb{R}^n$, the softmax function is Lipschitz continuous with respect to the Frobenius norm, which can be expressed as follows:

$$\|\text{softmax}(a) - \text{softmax}(b)\|_F \leq L_{\text{softmax}} \|a - b\|_F \quad (37)$$

Here, L_{softmax} is the Lipschitz constant of the softmax. Based on the derivations in the main text, we obtain the following expression:

$$\begin{aligned} \Delta A &= \text{softmax} \left(\frac{(q + \Delta q)(K + \Delta K)^\top}{\sqrt{d}} \right) \\ &\quad - \text{softmax} \left(\frac{q K^\top}{\sqrt{d}} \right) \end{aligned} \quad (38)$$

By jointly considering Equations 37 and 38, we can derive the following expression:

$$\|\Delta A\|_F \leq L_{softmax} \frac{\|(q + \Delta q)(K + \Delta K)^\top - qK^\top\|_F}{\sqrt{d}} \quad (39)$$

C Experimental Setup

Baselines We conduct extensive comparative evaluations against other pruning algorithms. LLM-Pruner (Ma et al., 2023) adopts structural pruning that selectively removes non-critical coupled structures based on gradient information. FLAP (An et al., 2024) is a structured pruning framework that reduces storage by leveraging fluctuation based metrics and adaptive model compression. Shortened LLaMA (Kim et al., 2024) selectively removes less important blocks based on block level importance scores, thereby accelerating model inference without significantly impacting performance. ShortGPT (Men et al., 2024) defines a BI metric to measure the importance of each layer within the model and directly removes those layers. SLEB (Song et al., 2024) employs a logit based approach to identify unnecessary transformer layers and updates the importance scores after each layer removal. SliceGPT (Ashkboos et al., 2024) is a post-training sparsification scheme which replaces each weight matrix with a smaller matrix. Through these comprehensive comparisons, we thoroughly assess the strengths of our approach.

Implementation Details Our experiments are conducted using the PyTorch framework (Paszke et al., 2019) and the Hugging Face Transformers library (Wolf et al., 2020). We use two nodes within the same local area network, with each node equipped with one NVIDIA H100 80GB GPU. We follow the respective compression strategies for prefill and decode as mentioned above. We set the parameter d_T to 0.95 by default. During the iterative block selection process, we initialize the annealing temperature T_0 at 15 to ensure sufficient exploration in the early stages. The temperature is then gradually reduced with a decay coefficient $\alpha = 0.85$ until it reaches the minimum temperature $T_{\min} = 0.05$. When distilling two blocks, we use the weights of the block with low cosine similarity as the initial weights. We distill the block using the PIQA and MMLU as the training set. The training is performed using the Adam optimizer with a learning rate of 1×10^{-5} , a batch size of 64 for 10 epochs. When sparsifying the KV Cache, we set the pruning ratio $p = 0.3$, with an attention

score threshold $\gamma = 0.75$ to preserve the most semantically important key value pairs. We set the performance improvement threshold mentioned in Section 3.3 to 3%. We conduct experiments with various hyperparameters to demonstrate the stability of our method. By default, we use 256 randomly sampled examples from PIQA and MMLU as the calibration set. In the zero shot performance comparisons, we maintain consistent experimental settings, including the calibration datasets.

D Experiments on Strong Scalability and Robust Generality (Larger Model, More Datasets and Additional Metric)

We further evaluate our method on the larger Qwen2.5-32B model with a pruning ratio of 25%. As reported in Table 8, our approach consistently achieves strong performance. Additionally, we report perplexity on WikiText2 using LLaMA2-13B and OPT-6.7B with pruning ratios of 24.37% and 20%, respectively, where our method achieves the best results (Table 9). Beyond these evaluations, we assess LLaMA3.1-8B-Instruct (Grattafiori et al., 2024) under a pruning ratio of 15.3% on two further benchmarks: the instruction-following dataset IFEval (Zhou et al., 2023a) and the code generation dataset HumanEval (Chen et al., 2021). As shown in Table 10, our method maintains strong performance across these tasks.

Method	PIQA	Winog	HSwag	ARC-E	ARC-C
Dense	81.88	75.3	64.91	80.51	53.41
LLM-Pruner	78.02	61.64	55.02	70.24	42.24
FLAP	77.56	61.08	55.23	70.36	42.37
Shortened	76.55	61.81	55.39	71.31	41.7
ShortGPT	76.66	72.53	52.4	72.85	42.24
SLEB	72.28	65.88	56.32	69.22	38.61
Ours	78.45	72.85	57	75.8	46.67

Table 8: Performance comparison of various methods on Qwen2.5-32B.

E Ablation Study

We conduct comprehensive ablation studies to evaluate the individual contributions of the key component of our framework: the iterative block removal strategy. We conduct experiments on LLaMA3.1-8B, involving the pruning of 9.38% blocks. The other hyperparameter settings used in these experiments are in the implementation details above. Block pruning performance, as shown in Figure 2, is significantly enhanced by the iterative optimi-

Model	Dense	LLM-Pruner	FLAP	Shortened	ShortGPT	SLEB	Ours
OPT-6.7B	10.86	11.92	11.68	12.51	13.68	12.94	11.28
LLaMA2-13B	4.88	8.16	9.73	10.81	9.25	8.96	7.38

Table 9: Evaluation of perplexity on WikiText2 for LLaMA2-13B and OPT-6.7B with pruning.

Benchmark	Dense	LLM-Pruner	FLAP	Shortened	ShortGPT	SLEB	Ours
IFEval	76.36	65.41	65.45	62.60	65.42	56.48	73.48
HumanEval	68.95	59.36	60.26	57.27	60.44	51.39	66.99

Table 10: Evaluation of LLaMA3.1-8B-Instruct under 15.3% pruning on IFEval and HumanEval.

mization mechanism, which consistently outperforms its non iterative counterpart. This advantage stems from the iterative strategy’s ability to more effectively navigate the search space, ultimately identifying superior block combinations that yield notable improvements in performance.

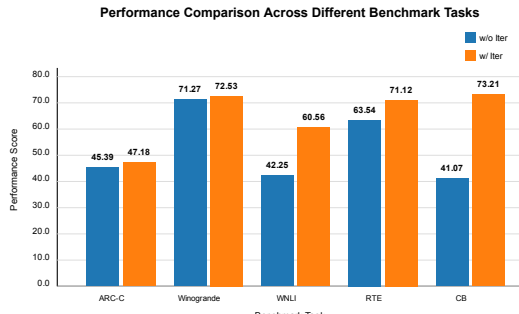


Figure 2: Ablation study on the effectiveness of the iterative block removal strategy: performance comparison with and without the strategy.

F Results of Different Pruning Ratios

Figure 3 illustrates the impact of different pruning ratios on LLaMA3.1-8B performance. As the pruning ratio increases, the accuracy of most tasks remains relatively stable despite a general downward trend, indicating the strong robustness of our method. Block pruning accuracy remains stable even when the number of pruned blocks increases, especially on tasks such as PIQA, Winogrande and RTE. This phenomenon validates the effectiveness of our redundancy aware iterative block pruning strategy, which selectively removes non-critical blocks while preserving the model’s core functional capabilities.

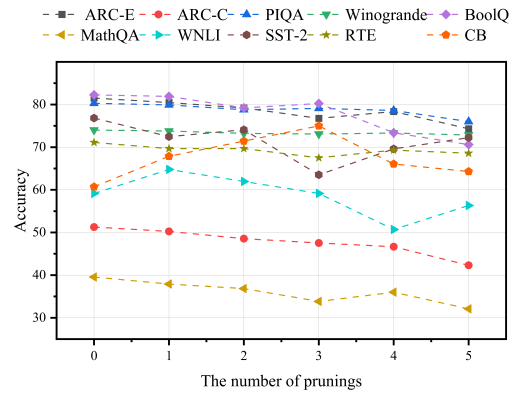


Figure 3: Results of model performance under different pruning blocks on LLaMA3.1-8B.

G Hyperparameter Impact Analysis

We evaluate the impact of key hyperparameters in our iterative block removal strategy, including the initial temperature T , temperature decay coefficient α , and minimum temperature T_{min} . We prune 9.38% blocks on LLaMA3.1-8B. As shown in Table 11, increasing T and α from the first configuration to the second configuration improves the average accuracy from 63.49 to 63.56. This indicates that a slower cooling schedule helps more effectively explore the solution space and avoid converging to suboptimal local minima. Importantly, further increasing the parameter values in the third configuration does not change the performance across all benchmarks, suggesting that the pruning process has converged. This convergence implies that the algorithm has identified a near optimal block removal combination, beyond which additional iterations or a larger search space will not yield further gains. Overall, all three configurations are able to find a high quality solution space.

T	α	T_{min}	ARC-E	ARC-C	PIQA	Winog	BoolQ	MathQA	WNLI	SST-2	RTE	CB	MMLU	CMMLU	HSwag	Avg
5	0.70	0.10	76.77	47.53	79.11	73.09	80.24	33.84	59.15	63.53	67.51	75.00	62.79	49.97	56.78	63.49
10	0.80	0.10	78.11	47.53	78.62	71.82	79.08	36.31	61.97	57.45	72.56	73.21	63.43	49.91	56.33	63.56
15	0.85	0.05	78.11	47.53	78.62	71.82	79.08	36.31	61.97	57.45	72.56	73.21	63.43	49.91	56.33	63.56

Table 11: Performance comparison across three key hyperparameter settings on the LLaMA3.1-8B. Under all these different parameter configurations, the model maintains a high level of performance.

d_T	ARC-E	ARC-C	PIQA	Winog	BoolQ	MathQA	WNLI	SST-2	RTE	CB	MMLU	CMMLU	HSwag	Avg
0.97	77.44	47.18	78.40	72.53	76.82	36.82	60.56	59.75	71.12	73.21	58.74	48.39	55.38	62.80
0.96	78.11	47.53	78.62	71.82	79.08	36.31	61.97	57.45	72.56	73.21	63.43	49.91	56.33	63.56
0.95	77.65	47.18	78.40	73.40	79.57	36.21	64.79	69.72	73.29	76.79	60.76	43.37	57.22	64.49
0.94	76.77	47.53	79.11	73.09	80.24	33.84	59.15	63.53	67.51	75.00	62.79	49.97	56.78	63.49

Table 12: Evaluation of the influence of the block distillation threshold d_T on the LLaMA3.1-8B.

Additionally, we further assess the threshold parameter d_T for constructing the distillation set. We prune 9.38% blocks of the LLaMA3.1-8B model. As shown in Table 12, the experimental results indicate that different threshold parameters can all achieve relatively optimal outcomes, consistently demonstrating good performance.

H Analysis of Iterative Block Removal Solutions

To validate the effectiveness of our iterative block removal method, we compare its solutions with the global optimum obtained via exhaustive search. It is important to note that exhaustive search requires evaluating all possible block combinations, which is practically intractable. To make this comparison feasible, we select all elements from the distillation set and the top five elements from the pruning set, and treat the optimal solution among all their combinations as the global optimum. Even so, solving it still demands substantial computational time. We apply our method to prune 13.6% of the parameters in LLaMA3.1-8B and evaluate it across various benchmarks. As shown in Table 13, our approach achieves results consistent with the global optimum. This demonstrates that our iterative method efficiently finds superior pruning solutions.

Method	PIQA	Winog	HSwag	ARC-E	ARC-C
Global Optimum	76.99	73.56	53.80	73.15	43.86
Ours	76.99	73.56	53.80	73.15	43.86

Table 13: Performance of iterative block removal compared to the global optimum on LLaMA3.1-8B.

I Analysis of Using Cosine Similarity

Besides cosine similarity, dot product and Euclidean distance are also commonly used, but they are sensitive to vector magnitude. Previous work (Chen et al., 2024) has shown that in Transformers, hidden states tend to expand with depth, leading deeper layers to exhibit higher dot-product similarity, while shallower layers maintain smaller Euclidean distances. To avoid this bias, we use cosine similarity, which is insensitive to magnitude. In addition, we measure the L2 norms of the hidden states at each layer of Qwen2.5-7B. As shown in Table 15, the norm magnitude exhibits a clear upward trend with increasing depth, which highlights the inherent bias of other similarity metrics that are sensitive to vector magnitude. Furthermore, we evaluate the performance of Qwen2.5-7B and OPT-13B under 15% parameter pruning with different similarity metrics. As shown in Table 14, cosine similarity consistently outperforms the other metrics.

Metric	PIQA	Winog	HSwag
Euclidean distance	75.70	52.20	50.51
Dot product	75.87	55.88	47.62
Cosine similarity	77.04	56.99	51.19

Table 14: Performance comparison on Qwen2.5-7B using different similarity metrics.

J Robustness on Different Calibration Sets

To evaluate the stability of our proposed block pruning strategy, we systematically analyze the consistency of results across different calibration sets

Layer	0	1	2	3	4	5	...	21	22	23	24	25	26	27
Norm	14	19	25	116	141	146	...	264	300	350	408	470	474	620

Table 15: The norms of the hidden states output at each layer of Qwen2.5-7B. The first row represents the layer IDs, and the second row represents the corresponding norms.

Calibration Set	Size	15.63% Blocks Removal	9.38% Blocks Removal
PIQA	256		
	512	24, 25, 26, [22, 23], [27, 28]	25, 26, [27, 28]
	1024		
WikiText-2	256		
	512	24, 25, 26, [22, 23], [27, 28]	25, 26, [27, 28]
	1024		

Table 16: Results comparison across different calibration sets. Under the LLaMA3.1-8B model, we report the selected block indices for removal across different calibration datasets and various sizes under two pruning configurations: removing 15.63% blocks and removing 9.38% blocks. The indices within square brackets denote the distilled blocks.

and sizes. Our analysis distinguishes between two types of removal operations: direct block pruning and block distillation. Direct block pruning refers to the removal of blocks, while block distillation involves merging blocks instead of removing them. As shown in Table 16, the experimental results demonstrate significant stability in the selection of removed blocks across all experimental conditions. This consistency strongly indicates that our pruning decisions are driven by the inherent architectural redundancy within the model itself, exhibiting robustness across different datasets.

K More Details on Prefill and Decode Removal Schemes

Our approach first determines the optimal removal strategy and then derives separate removal schemes for the prefill and decode stages. Specifically, the prefill scheme is designed as a subset of the decode scheme, ensuring that every retained block in the decode node can directly reuse the corresponding KV Cache from the prefill node. In contrast, if separate removal schemes are determined for the prefill and decode stages at the initial stage, without any subset relationship, it is likely that some blocks retained in the decode node would have no corresponding KV Cache in the prefill node, hindering cache reuse and reducing system efficiency.

L Comparison with Work of Similar Names

We compare our approach with another method (Muralidharan et al., 2024) that bears a similar name, as both involve concepts such as iteration and distillation. In their work, iteration refers to repeatedly performing pruning to gradually reduce the model size, whereas in our approach, iteration is used to search for the optimal pruning configuration, and the two notions are not directly related. Similarly, their distillation is applied after pruning to the entire model in order to restore performance, while our distillation occurs during the pruning process itself, serving as a mechanism for block removal.

M Case Study

To qualitatively assess the impact of pruning on generation quality, we compared the outputs of the original model and the pruned model for several representative prompts, as shown in Table 17. We prune 9.38% blocks on LLaMA3.1-8B. Despite a substantial reduction in model size, the pruned model consistently generates coherent, information-rich, and well-structured responses, retaining the core semantics of the original output. These examples confirm that our pruning strategy maintains strong generation capabilities and factual consistency even under significant structural compression.

Original Model	Pruned Model
<p><u>Explain what artificial intelligence is.</u> Artificial intelligence (AI) is the simulation of human intelligence processes by machines, especially computer systems. These processes include learning (the acquisition of information and rules for using the information), reasoning (using the rules to reach approximate or definite conclusions), and self-correction. Particular applications of AI ...</p>	<p><u>Explain what artificial intelligence is.</u> Artificial intelligence, or AI, is a field of computer science that deals with the creation of machines that can perform tasks that normally require human intelligence. This includes things such as understanding natural language, recognizing objects in images, and making decisions based on complex data. While AI has been around for decades, recent ...</p>
<p>Provide some tips for learning a new language.</p> <ol style="list-style-type: none"> 1. Set realistic goals: Start by setting realistic goals for yourself, such as learning a few basic phrases or mastering a specific skill. 2. Practice regularly: Consistency is key when it comes to learning a new language. 3. Find a language partner: Finding a language partner can be a great way to practice and improve your language skills. 4. Use technology... 	<p>Provide some tips for learning a new language.</p> <p>Here are some tips for learning a new language:</p> <ol style="list-style-type: none"> 1. Start by learning the basics of the language, such as the alphabet, common words and phrases, and basic grammar rules. 2. Find a language learning app or program that suits your learning style and goals. 3. Practice speaking and listening to the language as much as possible. 4. Practice ...
<p><u>Explain how a car engine works.</u> A car engine is a machine that converts the chemical energy stored in gasoline into mechanical energy that can be used to move the car. The engine consists of several parts that work together to produce this energy. The first part of the engine is the combustion chamber. This is where the gasoline is mixed with air and ignited to create an explosion. The explosion pushes down on a piston, which is connected to a crankshaft. The crankshaft is what turns wheels ...</p>	<p><u>Explain how a car engine works.</u> A car engine works by converting chemical energy stored in fuel into mechanical energy that drives the car. The process of converting chemical energy into mechanical energy is known as combustion. In a car engine, combustion occurs in the combustion chamber, which is located in the center of the engine. The combustion chamber is connected to the intake manifold, which is where the fuel and air mixture enters the engine. The intake manifold ...</p>

Table 17: Qualitative examples comparing outputs from the original and the pruned versions of the LLaMA3.1-8B models configured as described above. Each example illustrates the model’s response to the same input prompt, with the underlined text indicating the user’s question.